Chemical Engineering Journal 388 (2020) 124092

Contents lists available at ScienceDirect

Chemical Engineering Journal

journal homepage: www.elsevier.com/locate/cej

Additively manufactured packed bed device for process intensification of CO_2 absorption and other chemical processes

Eduardo Miramontes, Lonnie J. Love, Canhai Lai, Xin Sun, Costas Tsouris*

Energy and Transportation Science Division, Oak Ridge National Laboratory, Oak Ridge, TN 38831-6181, United States

HIGHLIGHTS

- Process-intensification packing device facilitates mass and heat transfer.
- 3D printed process-intensification device removes the heat of reaction.
- 3D printed structured packing heat exchanger is suitable for multiphase reactions.

GRAPHICAL ABSTRACT

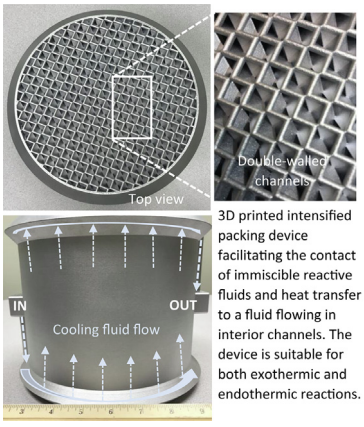

3D printed intensified packing device facilitating the contact of immiscible reactive fluids and heat transfer to a fluid flowing in interior channels. The device is suitable for both exothermic and endothermic reactions.

ARTICLE INFO

Keywords:
Carbon capture
Process intensification
Post-combustion absorption
Heat-exchanger reactors
3D printing
Structured packing

ABSTRACT

A 3D printed, structured packed-bed device has been developed to facilitate mass and heat transfer in multiphase-flow systems. This multifunctional device is compatible with commercially available packing elements used to effectively contact gas–liquid or liquid–liquid systems, and can be positioned along a packed bed to remove excess heat or supply thermal energy to a reactive system. The device is investigated for process intensification of CO_2 absorption by aqueous amines. The design, manufacturing, and functional characterization of the device are reported here. Its hydrodynamic properties are measured and compared to a polymer print of the same design. Pressure drop measurements are obtained for a dry system at various gas flow rates and also for an irrigated system at six liquid flow rates. The heat transfer properties of the process intensification device were explored by studying the behavior of the temperature profile inside the column for a gas only system before and after cooling. The behavior of the temperature profile was subsequently studied for an irrigated system. In order to better understand the physical behavior of the system, we developed a rigorous heat-transfer model using MFIX, a multiphase computational fluid dynamics software, and compared modeling results to experimental data. The overall heat transfer coefficient under various flow conditions was determined to be between 32 and 35 W/°C-m^2.

* Corresponding author.
E-mail address: tsourisc@ornl.gov (C. Tsouris).

https://doi.org/10.1016/j.cej.2020.124092
Received 18 October 2019; Received in revised form 8 January 2020; Accepted 10 January 2020
Available online 18 January 2020
1385-8947/

1. Introduction

1.1. Background

In 2018, global CO_2 emissions are estimated to have ballooned to an all-time high of 37.1 ± 1.8 Gt per year, a 2.7% increase from the previous year [1]. The hopes that global carbon emissions may have peaked from 2014 to 2016 have been dashed by the carbon budget reports from 2017 and 2018 which show that after three years of nearly no growth, emissions have once again continued to increase, by 1.7% in 2017 and 2.7% in 2018 [1]. These alarming trends underscore the urgency of developing viable mitigation strategies, if humanity is to achieve the Intergovernmental Panel on Climate Change (IPCC) target of preventing global average warming above 1.5 °C compared to pre-industrial levels. The ideal long-term solution is to replace fossil fuels with renewable energy, but the process will be lengthy; thus, it is essential to develop mitigation strategies in the interim. Carbon capture and storage (CCS) has been pursued as a viable short-term solution that targets power plant and industrial fossil fuel combustion emissions, which account for 46% of global carbon emissions [2].

There are several available CO_2 capture methods which can be categorized into pre-combustion, post-combustion, and oxy-fuel combustion capture using solvents, sorbents, membranes, CO_2 hydrate, and other materials and processes. Some of the methods investigated, however, are prohibitively costly, like cryogenic distillation, or in early development, like membrane diffusion. Absorption, on the other hand has an energy penalty second only to membrane diffusion capture, and is well understood, having been investigated since the 1970s. Moreover, it is easier to retrofit into existing facilities than the other technologies. These qualities have attracted considerable attention from researchers, and many consider absorption to be one of the most promising carbon capture technologies available [3]. The technology, however, has not yet been commercialized, as the energy penalty and cost remain far from economically viable. Further improvements to this technology are the subject of the current study.

This work explores and characterizes a device designed to optimize the capture efficiency of CO_2 absorption by process intensification. We build upon previous work [4], which characterized the metrics of the device for 3D printed polymer materials, to characterize the same metrics for a 3D printed aluminum device and expand the study of the device properties to the heat transfer domain. In addition, a mathematical model was developed to predict the temperature profile along the column and compare predictions to experimental data.

1.2. CO_2 absorption

Absorption processes separate CO_2 from flue gas by contacting it with a solvent whose chemical properties enable it to selectively capture CO_2. Aqueous solutions of alkanolamines such as monoethanolamine (MEA), diethanolamine (DEA), or diisopropanolamine (DIPA) are the most well attested solvents for carbon capture, but other families such as sterically hindered amines or ionic liquids have also been explored [5]. MEA is the preferred solvent because of its high absorption rate of CO_2 [6]. The absorption reaction between MEA and CO_2 can be represented by the following balanced reversible chemical equation [7]:

$$CO_2 + 2NH_2CH_2CH_2OH \leftrightarrow NHCH_2CH_2OH\text{-}COO^- + NH_2CH_2CH_2OH\text{-}H^+$$

To remove CO_2 from flue gas, CO_2-lean MEA solution is pumped into the top of an absorption column (absorber), where it flows countercurrently with flue gas. CO_2-rich MEA solution exits from the bottom and proceeds to a desorption vessel (desorber), where it is heated for regeneration. CO_2-lean MEA solution is then pumped back into the absorber. In this way, the solvent can be continuously recycled, which reduces operation costs.

1.3. Packed columns

Enhancing gas–liquid interactions significantly enhances mass transfer, so increasing the gas–liquid contact area per unit volume is a high priority. Packed columns are the most commonly employed technology for accomplishing this task. In addition to increasing contact area, they have a high gas capacity and a relatively low pressure drop. These properties make them desirable for carbon capture.

There are two different types of packed columns: those with structured packing and those with random packing. Random packing consists of small structures, typically rings or ring-like structures, that increase the surface area inside a packed column. The small structures are randomly distributed inside the column, hence the name. Examples include Raschig Rings, Pall Rings, and Dixon Rings. Structured packing typically consists of corrugated sheets designed to force fluids through defined paths. Examples include Mellapak 250, Sulzer BX, and Ralu Pak 250 [8]. Structured packing is generally preferred for carbon capture because it provides more effective interfacial contact area between gas and liquid phases [9].

1.4. Limitations of absorption

Despite being considered one of the least costly CO_2 capture methods, absorption still imposes a substantial energy penalty on a power plant. Gottlicher et al [10] reported the energy penalty as 0.341 kWh/kg CO_2. The largest component of the energy consumed by the process is in the regeneration of the solvent, a consequence of MEA's high heat of desorption. The energy required to pump the solvent and the energy required to compress CO_2 after it exits the desorber also consume significant amounts of energy. MEA undergoes thermal degradation due to the formation of oxazolidones and diamines. This risk limits the regeneration temperature to 120 °C which increases the heat duty of the reboiler and increases material costs by necessitating replacement of the solvent [5]. There will also be a pressure drop between the bottom of the column and the top due to the packing elements creating resistance to the flow of flue gas. The pressure drop will determine the size of the blower needed since a higher pressure drop means a blower has to work harder to achieve a given flow condition.

While MEA's relatively high reaction rate with CO_2 is desirable, it carries significant drawbacks. The forward reaction is thermodynamically favored under low temperature and high CO_2 partial pressure, and it is highly exothermic. Conversely, at high temperature and low partial pressure, the reaction reverses in the desorption direction, and is endothermic [11]. The reverse reaction is useful for regenerating the solvent; however, it presents a problem for absorption because if the reaction temperature increases, it can tip the balance toward desorption, thus inhibiting the absorption efficiency. This occurs during the absorption of CO_2 by MEA due to the highly exothermic character of the reaction. The heat released by the reaction can accumulate in the absorber and the temperature can rise to exceed 80 °C [12]. Previous studies have shown that at a temperature of 90 °C, 50% of the absorbed CO_2 is desorbed, and if the temperature rises further to 100 °C, 96% of the absorbed carbon is released [13].

It is evident from the preceding discussion that the thermodynamics of the MEA absorption reaction pose one of the most significant hurdles to the widespread adoption of amine absorption technology. However, this also presents an opportunity to vastly improve the energy efficiency of absorption technology by devising a method for dissipating heat generated by the reaction. Lower temperature will produce a higher CO_2 capture rate per unit energy.

Since technology that maximizes the contact area between MEA and CO_2, such as the aforementioned packed columns, is also pivotal to reaction efficiency, the ideal solution is one that can incorporate heat exchange into a packed column. It would also be desirable to dissipate

the heat *in situ* as it is generated, since increasing the distance between the reactor and heat removal would limit the cooling effect on the equilibrium of the reaction [14]. These conditions suggest that a possible solution would be to combine heat exchange and contact of phases into one stage. In chemical engineering, this can be characterized as a process intensification approach.

1.5. Process intensification

Process intensification emerged as a distinct trend in chemical engineering during the 1970s. A universal description remains elusive, however, size reduction of chemical plants, mitigation of environmental impact, improved energy efficiency, improved safety, and multifunctionality have all been identified as important facets [15]. Multifunctionality is of particular interest in light of the challenges posed by CO_2 absorption. The proposed solution is exactly this; the fusion of two separate functions, optimizing contact of phases and heat exchange, into a single device.

The combination of reaction and heat exchange has precedent in the literature, also dating back to the 1970s. One of the first examples of a heat exchanger-reactor (HEX) is a monolithic structure developed by Degnan and Wei [16]. The structure consisted of four monoliths composed of reaction channels deposited with pelleted catalysts sandwiched in between coolant channels arranged in series. The objective was to remove excess heat from the oxidation of CO, which is a highly exothermic reaction. This early example of HEX demonstrated the potential of the concept, as isothermal operation of the oxidation reaction was achieved by using a coolant stream running concurrently to the reactant stream [17].

More recently, a smaller variant of the design introduced by Degnan and Wei [16] called “micro-channel reactors” has been extensively studied. These small channel reactors have a higher surface area to volume ratio which enhances heat transfer and allows higher reaction rates. A prime example of this variant was developed by Bakhtiary-Davijany et al. to improve the efficiency of the synthesis of methanol from syngas [18]. This reaction is also highly exothermic which results in the formation of undesirable products. This modular heat exchanger reactor was composed of small reaction slits sandwiched in between cross flow oil channels. They were likewise able to achieve isothermal operation of the reaction, and it was found that the reaction channel temperature could effectively be controlled by the temperature of the heat transfer oil.

Other arrangements have been studied, such as a multi-channel heat exchanger reactor outlined by Guo et al. [19]. This reactor uses branching, or “arborescent” distributors that split into parallel channels as reactor channels. The parallel channels are suspended in a chamber where utility fluid is circulated to control the temperature. An evaluation of the flow distribution showed that it approaches uniformity which encourages good mixing properties. The total pressure drop was relatively low, but as the authors note, the geometry of their design is not optimized and could yield yet lower pressure drop. Most significantly, an application test on a sulfuric acid and sodium hydroxide neutralization reaction demonstrated that the reaction conditions could be effectively controlled by perturbing the flow rate of the coolant fluid. Isothermal operation was achieved for a highly exothermic neutralization reaction between sulphuric acid and sodium hydroxide.

These selected examples from the literature demonstrate that the heat exchanger reactor is a well attested concept, backed up by several decades of research. Not only have heat exchanger reactors been proven to be effective at cooling or heating the components of a reaction, but they have often enabled reactions to run isothermally. Guo et al. [19] showed that conditions could be controlled by variation of coolant fluid properties, which opens the possibility of thermostatic control of reaction conditions. Application of this technology to CO_2 capture has the potential to vastly improve the efficiency of carbon capture.

Most of the heat exchanger-reactors found in the literature, however, are modular structures typically consisting of corrugated foils or plates sandwiched together. This type of structure is unsuited to application in CO_2 absorption because it would be impractical to sandwich surfaces containing coolant channels in between the sheets of packed columns. There would be less space for solvent and flue gas than in an ordinary packed column of the same size, and the integrity of the packed column would likely be adversely affected. Recent advances in 3D printing, however, demonstrate that it is possible to incorporate elements such as flow channels without resorting to modular structures.

1.6. Additive manufacturing

Additive manufacturing, also known as 3D Printing or Rapid Prototyping, is a class of manufacturing technology that produces objects by depositing or sintering material in coordinates defined by digital modeling software. Additive manufacturing allows for seamless transition between a digital model and its physical realization. Commercial additive manufacturing technology contains software that automatically slices a 3D model into individual layers, the size of which is a limiting factor for the size of features, although layer thickness as small as 1 μm is possible with some kinds of printers [20]. These layers are then deposited by the printer and the object is built up layer by layer.

The layer-based construction and the seamless transition between modeling and physical object remove many of the fetters inherent in traditional manufacturing. Engineers are no longer limited by the kind of mold that can be built, or by the physical constraints of cutting tools. Almost anything that can be imagined and modeled using Computer Aided Design (CAD) can be manufactured, which gives engineers unparalleled design flexibility.

Additive manufacturing also allows for exotic geometries to be manufactured, such as the Schoen Gyroid, which can be used as a porous bed structure for an alternative heat exchanger design [21]. Such structures may have substantial advantages over conventional geometries, such as allowing for the geometry to be defined parametrically, but they are prohibitively difficult to manufacture by conventional means due to their internal labyrinthine structure. With the advent of additive manufacturing, these structures can now be explored.

One of the possibilities opened up by additive manufacturing is the ability to manufacture structures with embedded features. This ability has been used to great effect to streamline the production of electronics [22]. It can likewise be applied to chemical engineering by enabling engineers to embed channels for coolant flow in a mixer or reactor, thus eliminating the need to resort to modular structures. That capacity is the motivation for this study.

2. Materials and methods

2.1. Intensified device

The intensified packing device was designed at Oak Ridge National Laboratory’s Manufacturing Demonstration Facility and manufactured by Volunteer Aerospace LLC (Knoxville, Tennessee). Our approach is conceptually similar to previously developed HEX Reactors [11], in that it incorporates separate channels for reaction and heat exchange into the same device. However, rather than building the structure modularly by sandwiching etched sheets or stacking micro-structured plates together [11] the design versatility of 3D printing enables coolant channels to be integrated into a packing element.

The geometry of a Sulzer 250 Y packing element was used as a baseline for the design of a 3D printed monolith. These packing elements include surface roughness and perforations that were omitted for preliminary designs. Corrugated sheets were modeled in Solidworks and bundled together. The angle of corrugation can easily be altered, but for this study it was set to 45°. A cylindrical cut was then made on

the stack of corrugated sheets. Our previous studies have evaluated the hydrodynamic characteristics of 3D printed plastic packing elements of Mellapack geometry in comparison to those of metal and plastic commercial packing elements. It was found that 3D printed plastic packing elements had a pressure drop that compared favorably to both metal and plastic commercial packing elements; however, the wettability compared poorly to the metal commercial packing element which suggests selecting a more hydrophilic material would improve the performance of the device [4]. For that reason, as well as its high thermal conductivity, aluminum was chosen as the printing material in this study.

Internal coolant channels were subsequently added to the design of the device. The coolant fluid first flows around the perimeter of the device, then enters spaces within the baffles. Inside those spaces, the coolant channels run parallel to the corrugation angle, so that coolant flows counter-currently with the solvent, and co-currently with the gas. The inlet and outlet for the coolant were placed on the bottom and top of the device, respectively.

During testing of this first iteration of the intensified device, a leak was detected. Upon further investigation, the cause of the leak was discovered on the CAD file itself, where a 100-μm gap between the outer cylindrical enclosure and the coolant channel was found. The 3D printer was able to print this minute gap since its resolution is sufficiently low, which speaks to the ability of additive manufacturing to produce fine features.

2.2. Testing facility

The testing facility for the intensified device is a scaled down model of a real absorption column which can measure as much as 80 m in height and 20 m in diameter. The absorption column used to simulate plant-scale conditions was a 1-m tall, 8-in diameter column. At this scale, the residence time of the reactants is too short to allow sufficient heat to accumulate in the column, so cooling would have negligible benefits. To adequately simulate the properties of flue gas, fluids were delivered to the column at controlled temperatures using a thermostatically controlled Tutco Farnam Heat Torch 150 inline air heater for gas, and a thermostatically controlled Eemax Lavadvantage tankless water heater for solvent. A schematic of the experimental system is illustrated in Fig. 1.

The column consists of seven Mellapak 250 Y, 20.32 cm diameter commercial packing elements acquired from Sulzer, and the intensified

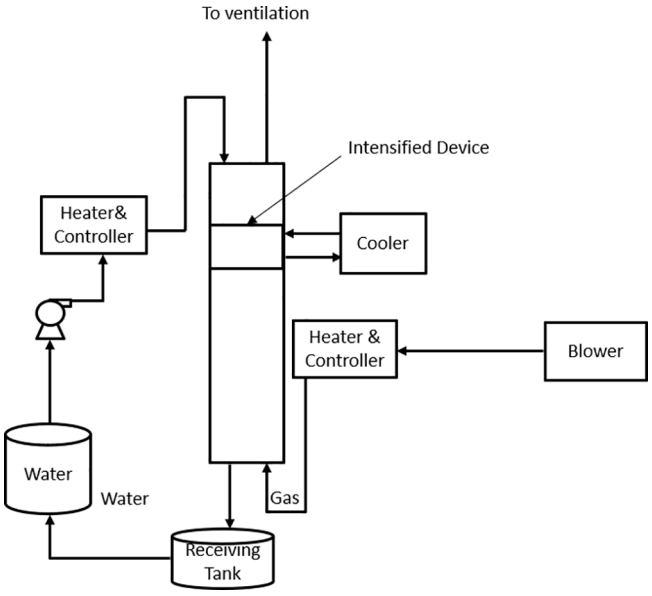

Fig. 1. Schematic of experimental system.

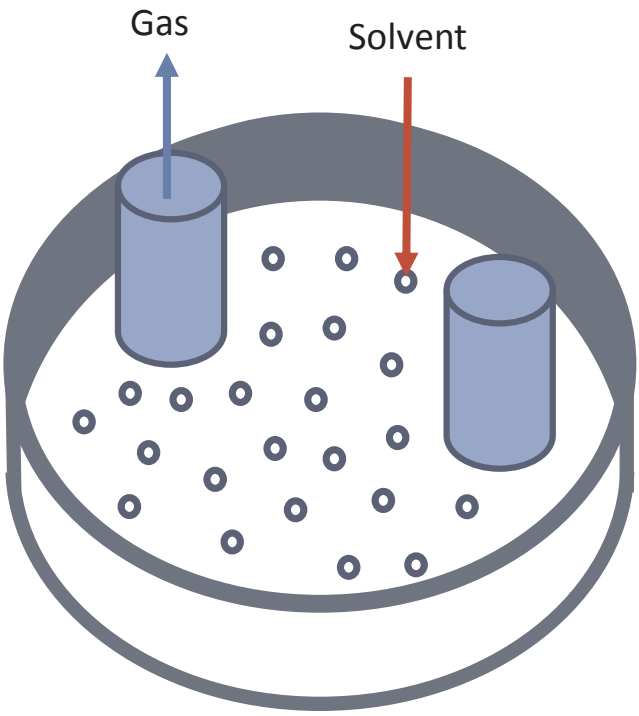

Fig. 2. Liquid distribution system.

device. The commercial packing elements are stacked

on top of each other, with the intensified device placed in the middle. This location was chosen because simulations using the MFIX multiphase computational fluid dynamics software [23] showed that this location would be where the largest accumulation of heat would be found, thus, cooling would yield the most noticeable results. For the purpose of testing heat transfer through the intensified device, air was delivered to the column from the bottom using a stainless-steel pipe in the shape of a T, with the air coming out of the sides of the pipe, to prevent water from entering the air lines. Water was pumped to the top of the column where it entered a liquid distribution system composed of a tray, punctuated with small holes of 1/8-inch diameter for water flow, and two plastic pipes for air to escape. A diagram of the liquid distribution system is shown in Fig. 2.

2.3. Data acquisition

Pressure drop across the intensified device was measured for both dry and irrigated systems using a handheld digital barometer. Gas flow was introduced to the system using a blower that allowed the flow rate to be controlled. Once the pressure reading stabilized, ten measurements were taken in 10 s intervals, and the average value was recorded. Liquid flow was then introduced into the system using a pump at 6 different flow rates, and pressure drop was measured as described. Wettability measurements were taken by submerging the device in water, then removing it, and determining the mass of water retained after 1) initial mild shaking, 2) further shaking, 3) additional shaking and drying of external surface, 4) and further shaking and drying of external surface. The mass of water retained was determined by subtracting the weight. The temperature of each fluid inside the column was measured *in situ* by type K thermocouples installed at four separate locations: at the very bottom of the column, immediately under the intensified device, immediately above the intensified device, and at the very top of the column. A diagram of the column internals including the packing element locations and measurement sites is shown in Fig. 3. Data recording software automatically recorded the temperature at each measurement site to generate a time dependent profile of the site.

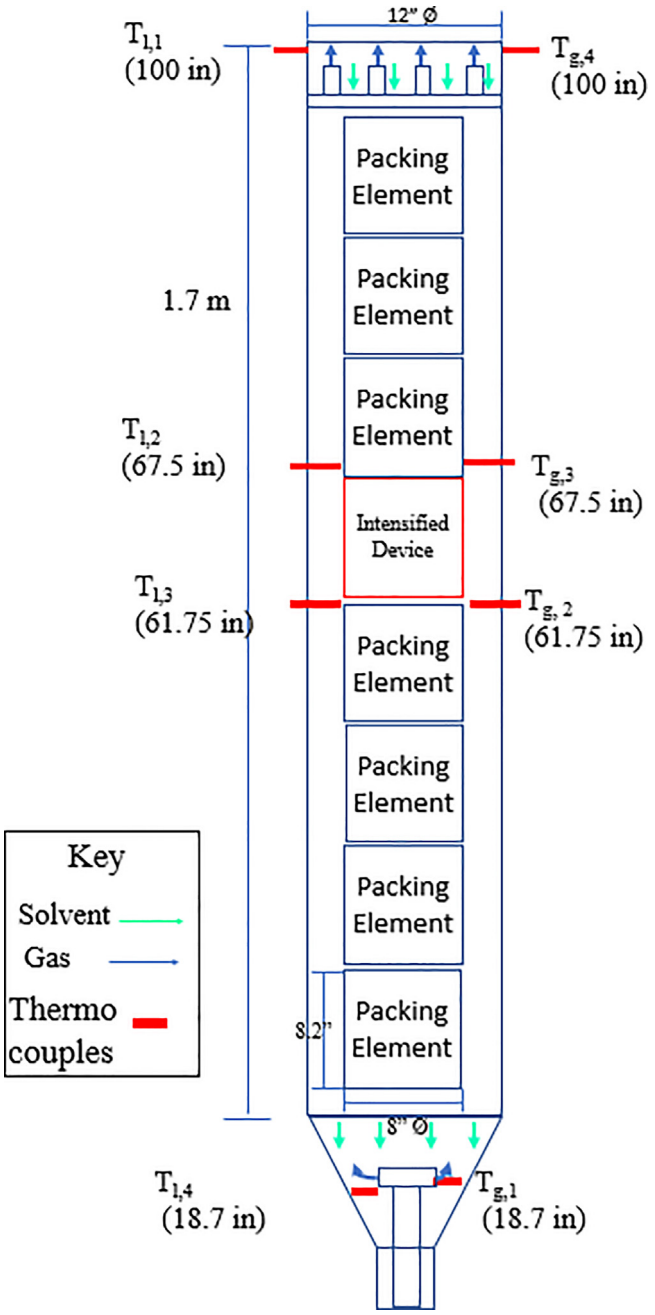

Fig. 3. Pilot scale absorption column and schematic of column internals.

Table 1
Flow and temperature conditions for irrigated experiments.

Case	Air Flow Rate (LPM)	Air Temperature (°C)	Water Flow Rate (LPM)	Water Temperature (°C)
1	650	60	1.36	80
2	650	60	1.81	80
3	650	60	2.26	80
4	650	60	2.26	60
5	650	60	2.26	40
6	520	60	2.26	80

The temperature of the air and water at each site was also recorded after the system reached steady state conditions for comparison of measurements with and without cooling.

First, the temperature profile of the column was studied using only air delivered to the system by a gas blower at 520 LPM, 650 LPM, and 780 LPM. The temperature of the input air was varied between 50 °C and 130 °C in intervals of 20 °C. Every set of conditions was repeated twice, once without cooling and once with cooling, and the resulting temperature profiles were contrasted with each other.

For dry system experiments the coolant was supplied by a 1345-W cooler manufactured by Thermo Fisher Scientific. Water was used as the coolant. The temperature set point of the coolant was 5 °C and the flow rate was held constant at 1.33 LPM.

Water was subsequently added to the column to study the behavior of the temperature profile in an irrigated system. The temperature profile of the absorption column was recorded at input air flow rate of 650 LPM and 520 LPM and input water flow rates of 1.36 LPM, 1.81 LPM, and 2.26 LPM. The temperature of the input air was 60 °C, and the water delivered to the system was heated to 40 °C, 60 °C, and 80 °C. The flow and temperature conditions for each experiment are tabulated in Table 1.

Due to power limitations, irrigated system experiments were conducted using a larger, 17.6 kW chiller manufactured by MultiAqua. The coolant was a 10% propylene glycol solution by volume. The chiller supplies a constant flow rate of 1.96 LPM. The temperature was set to 9 °C. The temperature of the coolant at the inlet and outlet of the intensified device were recorded using flow through temperature sensors connected to a handheld data logger.

2.4. Heat transfer analysis

The heat transfer rate of a fluid can be calculated using the measured flow rates, and measured temperatures at the inlet and outlet of the system using Equation (1):

$$q = \dot{m} c_p \Delta T$$

where q is the heat transfer rate (W), $\dot{m}$ is the mass flow rate of the fluid (kg/s), c_p is the specific heat capacity for water, and ΔT is the change in temperature between the inlet and outlet (°C). The specific heat capacity and density of water used to calculate the mass flow rate are taken from water property tables at the average temperature between the inlet and outlet [24].

The overall heat transfer coefficient, U, can be determined using the Log Mean Temperature Difference method if the heat transfer rate is known using the equation [25]:

$$U = \frac{q}{A \Delta T_{lm}} \tag{1}$$

where A is the contact surface area (m^2) and ΔT_{lm} is the log mean temperature difference (°C), given by:

$$\Delta T_{lm} = \frac{\Delta T_2 - \Delta T_1}{\ln(\frac{\Delta T_2}{\Delta T_1})} \tag{2}$$

Here, ΔT_1 and ΔT_2 are temperature differentials that depend on operating conditions. In the intensified device, the water is considered to flow co-currently with the coolant inside the device. Under co-current flow, temperature differentials are given by the following equations:

$$\Delta T_2 = T_{h,i} - T_{c,i} \tag{3}$$

$$\Delta T_1 = T_{h,i} - T_{c,o} \tag{4}$$

which give the difference in temperature between the hot fluid (solvent) and cold fluid (coolant) at the inlet and outlet.

The Log Mean Temperature Difference Method has several limitations. It can only be performed on two-phase systems, which excludes three-phase systems like an absorption column; therefore, one of the phases has to be neglected in the calculations. The heat transfer of the air was neglected in this case because of its much lower specific heat. Moreover, the method also assumes an adiabatic system, which does not hold for the absorption column as a substantial heat loss was

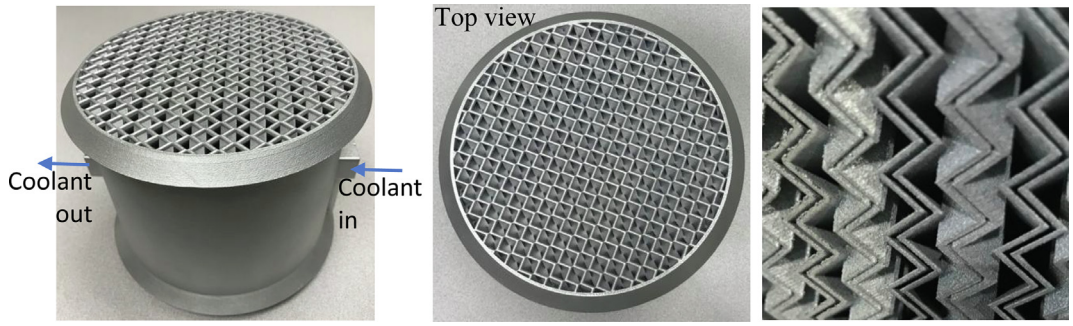

Fig. 4. Second generation aluminum intensified device. Left: 3D printed device; middle: top view; right: double-walled channels through which heat-transfer fluid flows (the difference in color is due to different roughness that can be controlled during printing to facilitate mixing).

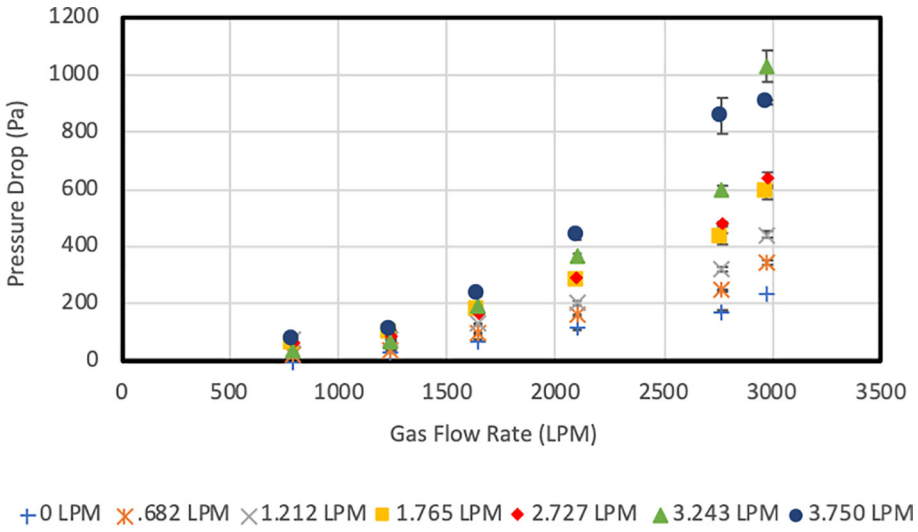

Fig. 5. Dry and irrigated pressure drop across aluminum intensified device.

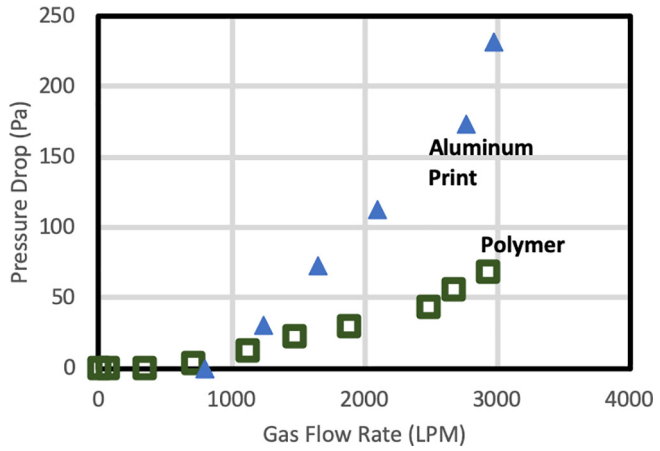

Fig. 6. Aluminum dry pressure drop measurements compared to polymer print dry pressure drop measurements obtained in Bolton et al. (2019).

observed even without cooling. The calculated heat transfer coefficient is therefore a combination of ambient cooling and cooling from the intensified device and should be considered a first order approximation.

2.5. MFIX simulations

A model of the absorption system with added cooling was developed using MFIX-TFM (Multiphase Flow with Interphase eXchanges) to aid in the design of intensified devices incorporated into an absorption column. The model will provide detailed knowledge of the physical and chemical properties of the system as a function of operating conditions which will be critical to designing a packed bed reactor and intensified devices to match at plant scale. The experimentally determined heat transfer coefficient for the intensified device will be input to the model to improve its accuracy, and the simulated temperature profile results will be compared to measured data to validate the model. The model will in turn be employed to shed light on the dynamics of absorption and to predict the behavior of the system in reactive experiments. In this paper, the model will be used to simulate the nonreactive system at the operating conditions tabulated in Table 1.

MFIX is an open source multiphase flow modeling tool developed at the National Energy Technology Laboratory (NETL), and the MFIX -TFM (Two-Fluid Model) is an Eulerian-Eulerian model which supports a broad range of capabilities for dense, reacting, multiphase flows by representing the fluid and solids as interpenetrating continua [23] (see description in Supporting Information). The MFIX model of solvent absorption, a custom extension of the MFIX-TFM model that models liquid and gas two phase flow [26–28] has been used in the current effort for validation purposes for the irrigated system experiments. In this gas–liquid MFIX-TFM, the coupling of hydrodynamics for countercurrent gas–liquid flow through a packed column, chemical reactions, and heat and mass transfer specific to CO_2 absorption using MEA has been modeled. In applying this gas–liquid MFIX TFM, the model parameters have been carefully chosen so that the two-phase pressure drop, liquid holdup, wetting efficiency, and mass transfer efficiency as a function of operating conditions are either matching with the experiment data or existing literature reports. The cooling from the coolant flow in the intensified device has been modeled as heat transfer with a

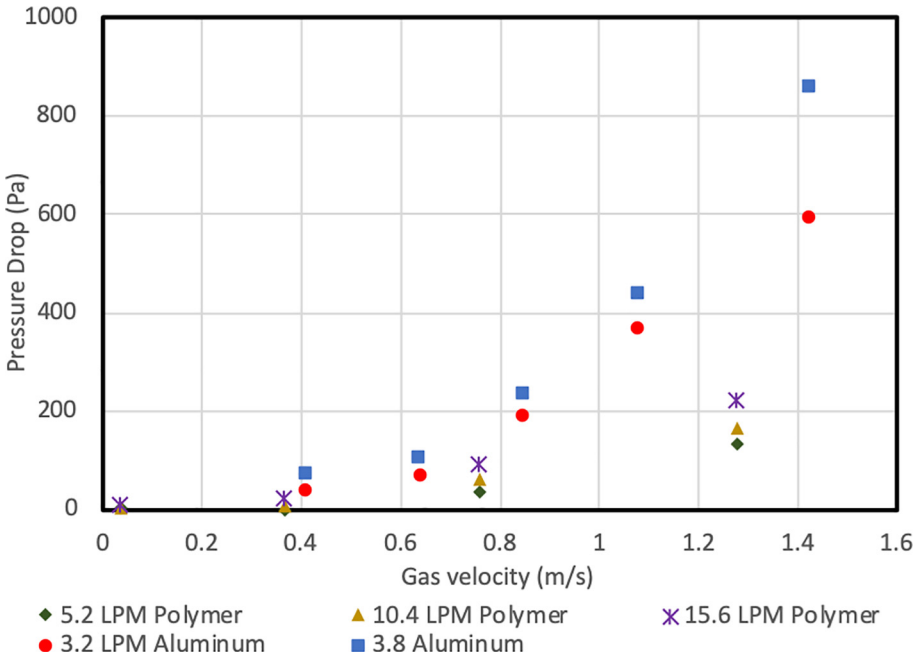

Fig. 7. Comparison of irrigated pressure drop between aluminum print and polymer print.

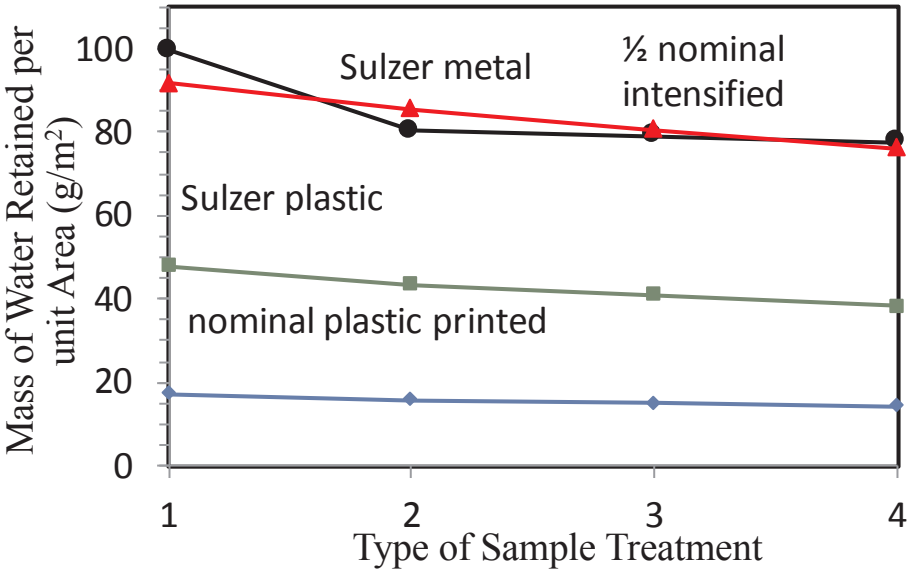

Fig. 8. Wettability measurements per surface area of aluminum intensified device print compared to measurements for Sulzer plastic prints obtained by Bolton et al. (2019). (o) Sulzer metal. (Δ) ½ nominal intensified. (□) Sulzer plastic (◊) Nominal plastic printed.

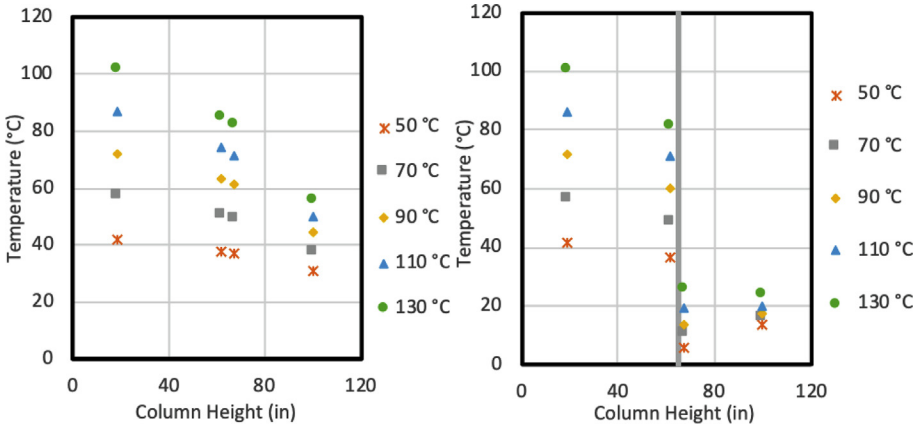

Fig. 9. Dry system temperature profiles inside the absorption column at various input gas temperatures for gas flow rate of 650 LPM. Left: without cooling. Right: with cooling. Gray line spans the height of intensified device.

Table 2
Change in temperature of air flowing through intensified device for different flow rate conditions at input temperature of 130 °C.

Flow Rate (LPM)	$T_{1,2}$ (°C)	$T_{1,3}$ (°C)	ΔT (°C)
520	75.8	14.1	61.7
650	81.7	25.7	56.0
780	86.2	37.9	48.3

fixed temperature coolant at a constant heat-transfer coefficient in the section where the intensified device is located. In addition, a uniform heat transfer coefficient along the column height has been applied to model the heat loss to the ambient air for this column with less than an ideal insulation. In the current work, the gas flow does not include any CO_2 and thus no chemical reaction is involved.

3. Results and discussion

3.1. Intensified device

The second-generation device, shown in Fig. 4, solved the leaking problem observed in the first generation. The gap discovered in the CAD file was sealed and the design was altered to move the inlet and outlet to the sides of the device for convenience in mounting. Additionally, the external surface of the channels was smoothed into a semi-circular shape to reduce pressure drop. Subsequent tests revealed no further leaks up to a pressure of 137.9 kPa across the wall, and it was concluded that the second-generation aluminum print is suitable for hydrodynamic and carbon capture studies. The device measures 20.3 cm in diameter and 14.6 cm in height, and the volume of liquid necessary to fill up the internal channels was measured to be 650 mL. The total packing surface area of the device is 2.671 m^2, and the total thickness of each wall including the two solid sides and the gap in between is approximately 3 mm. It is estimated that the gap thickness is approximately 1 mm. Hydrodynamic and heat transfer analyses of the second-generation device are detailed in the remainder of this section.

3.2. Pressure drop

The results of the pressure drop experiments are shown in Fig. 5. Each data point represents the average of 10 measurements. The standard deviation of the measurements was taken and represented as error bar. The standard deviation was negligible in most data points except for the two points with the highest flow rates. As expected, the dry pressure drop measurements were the lowest, and the pressure drop

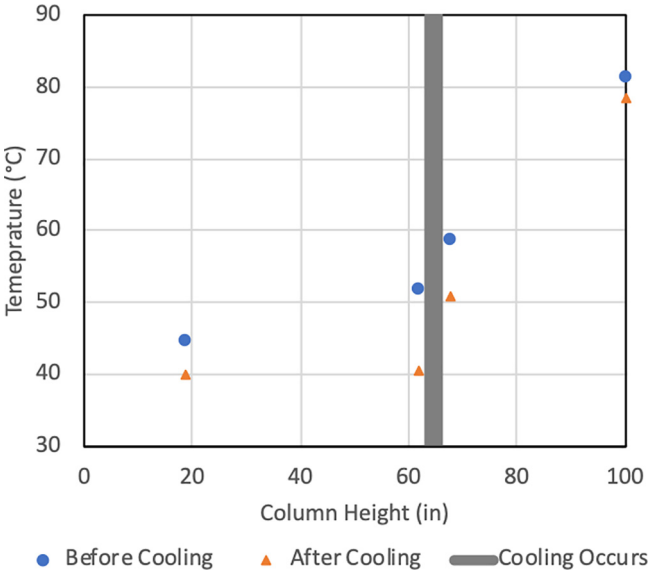

Fig. 11. Typical results of heat transfer experiments in an irrigated column. Conditions shown are input air at 650 LPM and 80 °C. Water flows at 2.26 LPM and 80 °C.

Table 3
Heat transfer coefficient for various flow and temperature conditions.

Air Flow Rate (LPM)	Air Temperature (°C)	Water Flow Rate (LPM)	Water Temperature (°C)	Heat Transfer Coefficient (W/K-m^2)
650	80	1.36	80	34.7
650	80	1.81	80	34.7
650	80	2.26	80	32.8
650	80	2.26	60	32.8
650	80	2.26	40	32.5
520	80	2.26	80	34.9

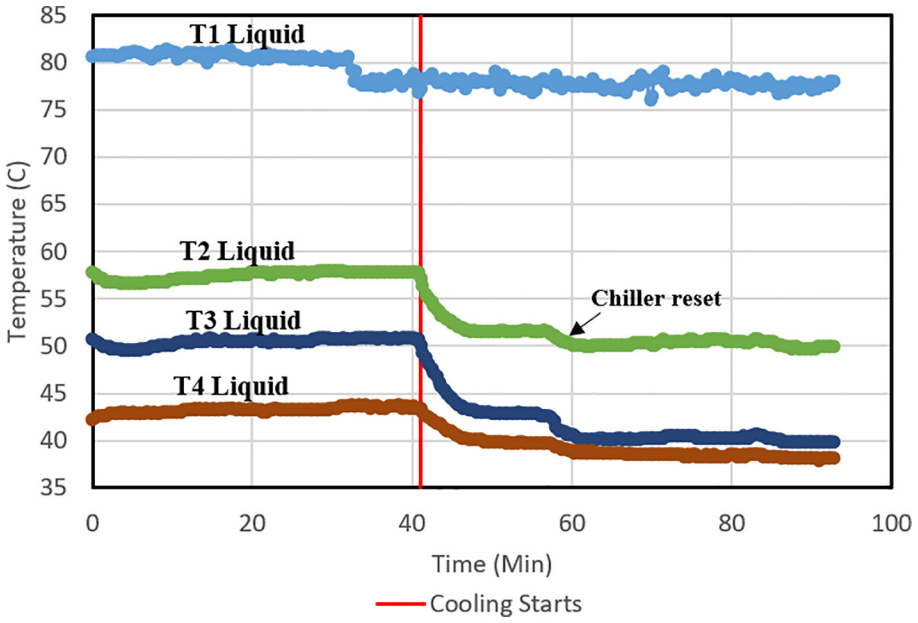

Fig. 10. Transient temperature profile of irrigated system before and after cooling. Cooling was turned on at 40 min.

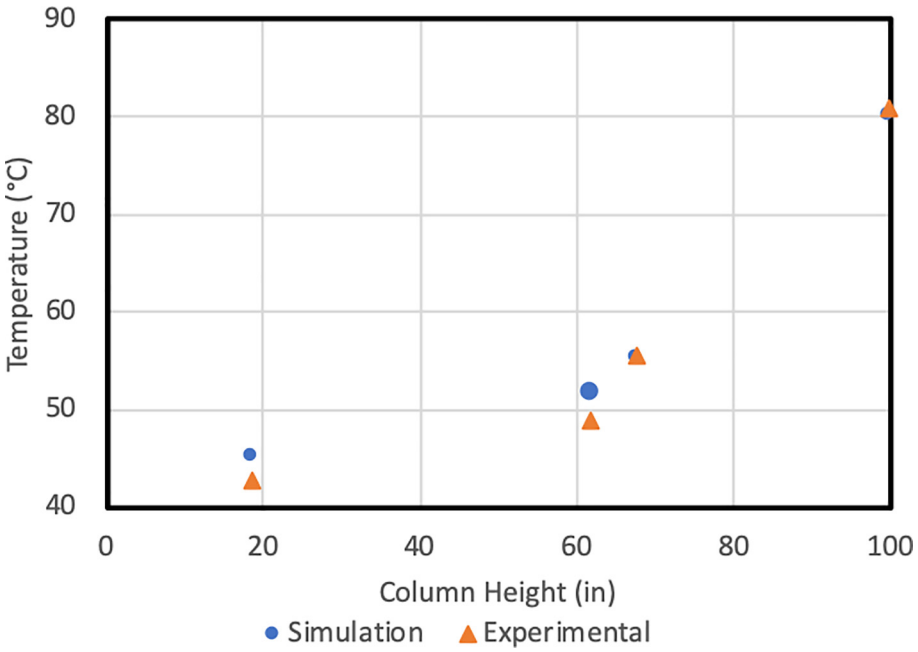

Fig. 12. Comparison of uncooled liquid temperature profile between MFIX simulation and experimental results.

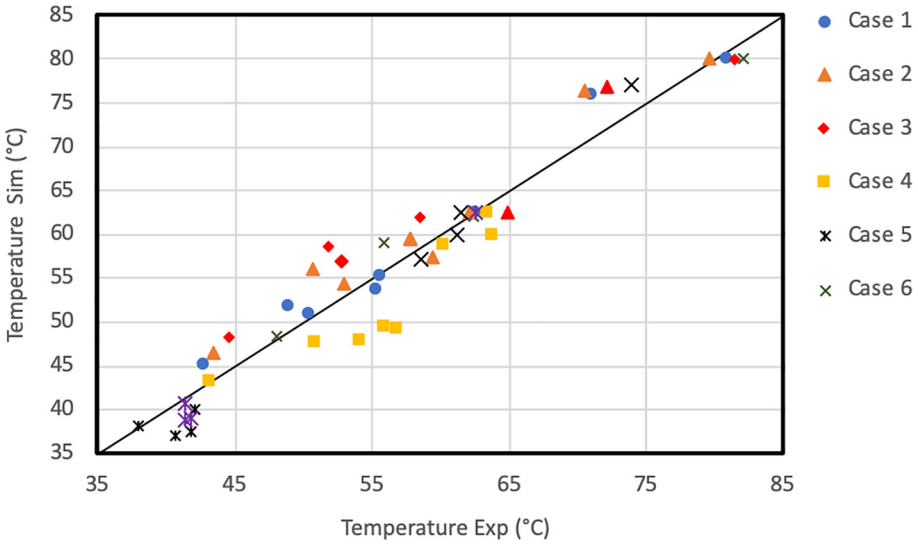

Fig. 13. Parity plot for Uncooled Air-H_2O system. Experimental vs simulated by the MFIX Model.

increases with increasing liquid flow rate. The behavior of the pressure drop compares well to Mackowiak's model, as the expected exponential rise in pressure drop near flooding was observed [6]. The data point corresponding to the highest gas and water flow rates, however, did not rise as expected, which likely occurred because of air leak developed through the wall of the column due to the high airflow rate.

The dry pressure drop of the aluminum print was compared with that of the polymer print of identical geometry from Bolton et al. in Fig. 6. The pressure drop was higher for the aluminum print, which agrees with the findings of Bolton et al. [21], where the pressure drop through a metal Mellapak 250 Y packing element was found to be higher than pressure drop of plasticelements.

A comparison was also made between the aluminum print and polymer print for irrigated pressure drop, which is shown in Fig. 7. Here again, the pattern from the dry pressure drop comparison holds, and the aluminum print exhibits a higher pressure drop than the polymer, even at much lower flow rates. The difference appears to be greater than the difference observed in the dry pressure drop comparison, due to the much lower water flow rates used in the aluminum print measurements. The higher pressure drop observed for the intensified device can be reduced by increasing the size of the unit cell, or decreasing the surface area of the device.

3.3. *Wettability*

The wettability of the aluminum print was measured and compared to the results for Sulzer 250 packing elements and simple 3D printed plastic elements acquired in the previous phase of the project by Bolton et al. [21]. The comparison is shown in Fig. 8. The type of sample treatment refers to the method described in Section 2.2. The mass of water retained by the 3D printed aluminum print closely resembles the results obtained for the Sulzer Mellapak 250 Y stainless steel packing element which suggests the hydrophilicity of metal is not adversely affected by the printing process. These results validate the decision to print the intensified device using aluminum, since higher wettability enhances contact between gas and liquid phases.

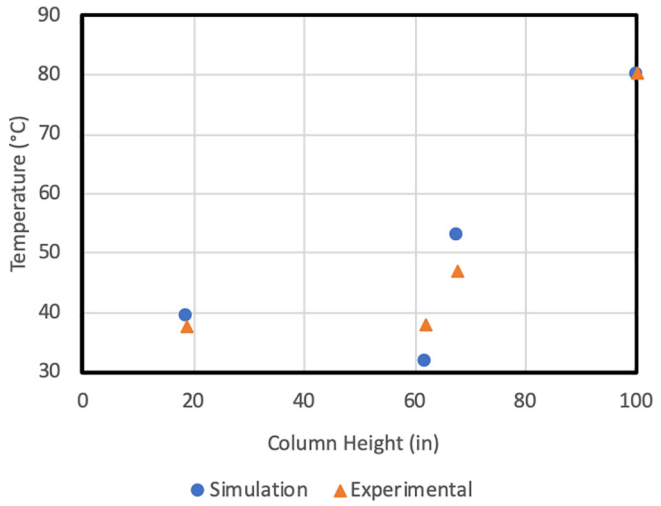

Fig. 14. Comparison of cooled temperature profile between MFIX simulation and experimental results.

3.4. Temperature profile

A sample comparison of temperature profiles for the dry system without cooling (left) and with cooling (right) at 650 LPM is shown in Fig. 9. A significant drop in temperature was exhibited by the system without cooling due to heat losses to the environment, with higher heat losses being observed for higher input air temperatures, as high as 100 °C for input air at 130 °C. Nevertheless, the addition of cooling drastically reduced the temperature of the column above the intensified device, with a post cooling temperature reduction as high as 61.7 for 520 LPM. The post-cooling temperature reduction, defined as change from $T_{g,2}$ to $T_{g,3}$, for other gas flow rates is shown in Table 2. The substantial difference in the temperature profile after cooling demonstrates the ability of the intensified device to act as a heat exchanger.

A sample transient profile of the liquid temperatures for the irrigated system is shown in Fig. 10. The input air flow rate was 650 LPM and its temperature was 60 °C, while the water flow rate was 1.81 LPM and it was heated to 60 °C. The coolant fluid was cooled to 9 °C, however, it was measured to be 19 °C at the inlet of the intensified device. This discrepancy is thought to be caused by the chiller lacking the power to cool the fluid all the way back to the set point. The moment that cooling was activated is demarcated on the temperature profile by a red line. The impact of cooling in this case is less drastic than for air, which is expected on account of the much higher heat capacity of the heated water. Nevertheless, a significant reduction in temperature post-cooling was observed. The temperature at $T_{l,3}$ was reduced by 11 °C. Interestingly, the temperature at $T_{l,2}$ was reduced by 8 °C, despite this location being above the intensified device.

The geometric temperature profile of the water inside the column is presented in Fig. 11 for three different water flow rates. All three experiments were conducted with input air at 80 °C and 650 LPM, and input water at 80 °C. The temperature profile of the gas closely followed that of the water, as both phases were in intimate contact, so only the liquid temperature is shown. This result demonstrates that with appropriately sized cooling equipment, the intensified device can have strong heat-exchange capability. The results, however, also reveal that the water is losing large amounts of heat even prior to the cooling, which limits the ability of the experiments to demonstrate the benefit of cooling. There are two likely culprits for this behavior. One is heat losses to ambient, and the other is vaporization of the liquid phase into the gas because of the low humidity air being pumped into the column, which would remove heat from the liquid and reduce the temperature of the system. Despite this limitation, these results demonstrate that the intensified device is a viable heat-exchange device when water is added to the system.

3.5. Overall heat transfer coefficient

The overall heat transfer coefficient at various experimental conditions is presented in Table 3. Overall, the calculated values exhibit very good agreement with each other and only vary between 32.5 and 34.9 W/°C-m^2. The consistency in the results indicate a well behaving system. Changes in flow rate had a very small effect on the overall heat transfer coefficient, which could be a consequence of the small variation in flow rate—an interval of only 0.45 LPM between each flow rate. For liquid–liquid heat exchange, the overall heat-transfer coefficients can range from 150-2000 W/m^{2}K, while for gas–liquid heat exchange, the overall heat-transfer coefficients can range from 15 to 70 W/m^{2}K [25].

3.6. Modeling

The experimental heat transfer data were compared to temperature profiles predicted by MFIX at the same temperature and flow conditions. A comparison of the experimental and simulation temperature profiles for Case 1 without cooling is shown in Fig. 12.

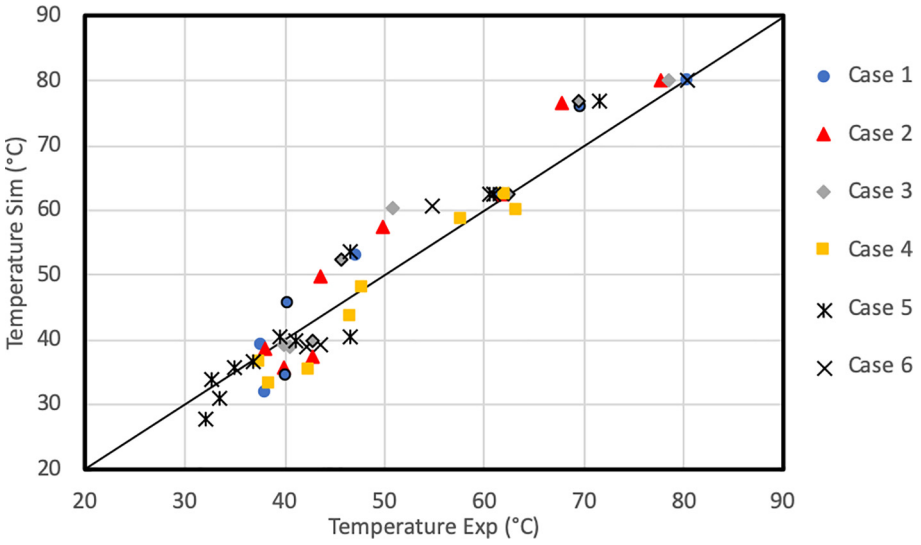

Fig. 15. Parity plot for Cooled Air-H_2O system. Experiment vs simulated by the MFIX Model.

The concordance between experimental and simulated temperature profiles is remarkably good. The accuracy of MFIX predictions for the rest of the uncooled cases was similarly satisfactory as the relative deviation from experimental results was between 0 and 14%, with most well under 10%. A comparison between experimental and simulation results for all data points is presented in a parity plot, shown in Fig. 13. The cases shown in the plot are the ones outlined in Table 1. The parity plot demonstrates the accuracy of the model at various experimental conditions, for both air and gas, as the data do not stray far from the perfect parity line.

Simulations that incorporated cooling by the intensified device were also performed on MFIX. A comparison between the simulated and experimental cooled temperature profile is again shown for Case 1 in Fig. 14. The accuracy of the MFIX predictions is still reasonably good although less so than for the uncooled case. The simulation successfully predicted the final value of the liquid temperature profile (at the lowest point), but deviated for the two middle values. The remaining cooled cases demonstrate a similar pattern; there is a wider spread in the relative deviation from measured values for cooled cases which ranged from 0 to 19%. A comparison of all cooled cases is presented in a parity plot, shown in Fig. 15.

4. Conclusions

An intensified packing device to simultaneously enhance contact between two reacting process fluids and heat transfer between the two process fluids and a third (cooling/heating) fluid has been additively manufactured successfully and demonstrated in this study. The pressure drop measurements obtained for the additively manufactured aluminum intensified device print followed the behavior described by Mackowiak's model, and the expected exponential rise in pressure drop near flooding was observed. The dry pressure drop was higher in the aluminum print than in the polymer print which confirms the results of earlier studies. The irrigated pressure drop was higher as well; however, one possible way to mitigate the increased pressure drop may be to increase the unit cell size of the device or reduce the surface area. Wettability measurements revealed that the aluminum intensified device compares favorably to metal Mellapak 250 Y commercial packing elements. Wettability is an important parameter that influences the ability of the device to enhance gas and liquid phase interactions; consequently, these results, in addition to aluminum's high thermal conductivity which will enhance heat transfer, vindicate the decision to manufacture the device out of aluminum. Future research, however, may focus on identifying materials with an even more desirable combination of wettability and heat conductivity.

Preliminary experiments on heat transfer have demonstrated the effectiveness of cooling which can be observed in the dramatic temperature reduction achieved in gas that flowed through the intensified device, which was as high as 61.7 °C for 520 LPM. For some gas flow rates, the entire top half of the column was held close to room temperature even at input gas temperatures exceeding 100 °C because of heat losses through the wall. As expected, the effect of the cooling was less dramatic in the irrigated system than in the air alone system due to water's higher heat capacity, as well as vaporization of water into air that reduces the temperature of the whole system; nevertheless, cooling still had a measurable impact and was able to reduce the temperature of the water by up to 11 °C. The heat transfer coefficient of the irrigated system under the tested conditions exhibited close agreement between different flow rates and varied between 32.5 and 34.9 W/°C-m^2.

The experimental heat transfer data from the irrigated system were tested against a rigorous model developed in MFIX. Both cooled and uncooled simulated temperature profiles exhibited close concordance to experimental data which validates the efficacy of the MFIX model for predicting the thermal behavior of irrigated absorption columns. Future work could explore the ability of the model to predict the thermal behavior of an MEA-CO_2 absorption system.

Declaration of Competing Interest

The authors declare that they have no known competing financial interests or personal relationships that could have appeared to influence the work reported in this paper.

Acknowledgments

This research was funded by the Office of Fossil Energy of the U.S. Department of Energy. Technical help by Scott Palko, John Storey, and James Parks II of the Applied Catalysis & Emissions Research Group is gratefully acknowledged. The authors are also thankful to Mr. Jonaaron Jones and his group with Volunteer Aerospace LLC for printing the intensified packing device.

Appendix A. Supplementary data

Supplementary data to this article can be found online at https://doi.org/10.1016/j.cej.2020.124092.

References

[1] C. Le Quéré, et al., Global carbon budget 2018, Earth Syst. Sci. Data 10 (2018) 2147–2194, https://doi.org/10.5194/essd-10-2141-2018.
[2] Intergovernmental Panel on Climate Change, Drivers, Trends and Mitigation, Climate Change 2014 Mitigation of Climate Change. (n.d.) 33–111. 10.1017/cbo9781107415416.011.
[3] D. Aaron, C. Tsouris, Separation of CO_2 from flue gas: a review, Sep. Sci. Technol. 40 (2005) 321–348, https://doi.org/10.1081/ss-200042244.
[4] S. Bolton, A. Kasturi, S. Palko, C. Lai, L. Love, J. Parks, et al., 3D printed structures for optimized carbon capture technology in packed bed columns, Sep. Sci. Technol. 54 (2019) 2047–2058, https://doi.org/10.1080/01496395.2019.1622566.
[5] J. Oexmann, A. Kather, S. Linnenberg, U. Liebenthal, Post-combustion CO_2 capture: chemical absorption processes in coal-fired steam power plants, Greenhouse Gases: Sci. Technol. 2 (2012) 80–98, https://doi.org/10.1002/ghg.1273.
[6] A. Aroonwilas, A. Veawab, Characterization and comparison of the CO_2 absorption performance into single and blended Alkanolamines in a packed column, Ind. Eng. Chem. Res. 43 (2004) 2228–2237, https://doi.org/10.1021/ie0306067.
[7] B. Han, C. Zhou, J. Wu, D.J. Tempel, H. Cheng, Understanding CO_2 capture mechanisms in aqueous Monoethanolamine via first principles simulations, J. Phys. Chem. Lett. 2 (2011) 522–526, https://doi.org/10.1021/jz200037s.
[8] J. Mackowiak, C. Hall, Fluid Dynamics of Packed Columns Principles of the Fluid Dynamic Design of Columns for Gas/Liquid and Liquid/Liquid Systems, Springer, Berlin, Berlin, 2013.
[9] J.T. Yeh, H.W. Pennline, K.P. Resnik, Study of CO_2 absorption and desorption in a packed column, Energy Fuels 15 (2001) 274–278, https://doi.org/10.1021/ef0002389.
[10] G. Gottlicher, R. Pruschek, Comparison of CO_2 removal systems for fossil-fuelled power plant processes, Energy Convers. Manage. 38 (1997) S173–S178, https://doi.org/10.1016/S0196-8904(96)00265-8.
[11] A. Veawab A. Aroonwilas A. Chakma P. Tontiwachwuthikul Solvent Formulation for CO2 separation from flue gas streams. University of Regina. S4S 0A2.
[12] H.M. Kvamsdal, G.T. Rochelle, Effects of the temperature bulge in CO_2 absorption from flue gas by aqueous monoethanolamine, Ind. Eng. Chem. Res. 47 (2008) 867–875, https://doi.org/10.1021/ie061651s.
[13] W.-J. Choi, J.-B. Seo, S.-Y. Jang, J.-H. Jung, K.-J. Oh, Removal characteristics of CO_2 using aqueous MEA/AMP solutions in the absorption and regeneration process, J. Environ. Sci. 21 (2009) 907–913, https://doi.org/10.1016/s1001-0742(08)62360-8.
[14] Z. Anxionnaz, M. Cabassud, C. Gourdon, P. Tochon, Heat exchanger/reactors (HEX reactors): concepts, technologies: state-of-the-art, Chem. Eng. Process.: Process Intensif. 47 (2008) 2029–2050, https://doi.org/10.1016/j.cep.2008.06.012.
[15] Y.-H. Kim, L.K. Park, S. Yiacoumi, C. Tsouris, Modular chemical process intensification: a review, Annu. Rev. Chem. Biomol. Eng. 8 (2017) 359–380, https://doi.org/10.1146/annurev-chembioeng-060816-101354.
[16] T.F. Degnan, J. Wei, Monolithic reactor-heat exchanger, ACS Symp. Ser. Chem.

React. Eng.—Houston (1978) 83–97, https://doi.org/10.1021/bk-1978-0065.ch008.
[17] T.F. Degnan, J. Wei, The Co-current reactor-heat exchanger part II, Exp. Results, AIChE J. 26 (1980) 60–67, https://doi.org/10.1002/aic.690260111.
[18] H. Bakhtiary-Davijany, F. Hayer, X.K. Phan, R. Myrstad, H.J. Venvik, P. Pfeifer, et al., Characteristics of an integrated micro packed bed reactor-heat exchanger for methanol synthesis from syngas, Chem. Eng. J. 167 (2011) 496–503, https://doi.org/10.1016/j.cej.2010.08.074.
[19] X. Guo, Y. Fan, L. Luo, Multi-channel heat exchanger-reactor using arborescent distributors: a characterization study of fluid distribution, heat exchange performance and exothermic reaction, Energy 69 (2014) 728–741, https://doi.org/10.1016/j.energy.2014.03.069.
[20] C. Parra-Cabrera, C. Achille, S. Kuhn, R. Ameloot, 3D printing in chemical engineering and catalytic technology: structured catalysts, mixers and reactors, Chem. Soc. Rev. 47 (2018) 209–230, https://doi.org/10.1039/c7cs00631d.
[21] C. Fee, 3D-printed porous bed structures, Curr. Opin. Chem. Eng. 18 (2017) 10–15, https://doi.org/10.1016/j.coche.2017.07.003.
[22] D. Espalin, D.W. Muse, E. Macdonald, R.B. Wicker, 3D printing multifunctionality: structures with electronics, Int. J. Adv. Manuf. Technol. 72 (2014) 963–978, https://doi.org/10.1007/s00170-014-5717-7.
[23] W. Wagner, A. Pruß, The IAWPS formulation for the thermodynamic properties of ordinary water substance for general and scientific use, J. Phys. Chem. Ref. Data 31 (2002) (1995) 387–535, https://doi.org/10.1063/1.1475333.
[24] T. Kuppan, Heat Exchanger Design Handbook, CRC Press, Boca Raton, 2017.
[25] K.M. Lunsford, Increasing heat exchanger performance, Bryan Research & Engineering Inc, 1998.
[26] J.E. Carney J.R. Finn Device Scale Modeling of Solvent Absorption using MFIX-TFM 2016 10.2172/1350958.
[27] W.E. Ranz, W.R.J. Marshall, Evaporation from drops: Part II, Chem. Eng. Prog. 48 (1952) 173–180.
[28] D. Gunn, Transfer of heat or mass to particles in fixed and fluidised beds, Int. J. Heat Mass Trans. 21 (1978) 467–476, https://doi.org/10.1016/0017-9310(78)90080-7.